Thermodynamically Induced Transport Anomaly in Dilute Metals $ZrTe_5$ and $HfTe_5$

Chenjie Wang*
Department of Physics and HKU-UCAS Joint Institute for Theoretical and Computational Physics, The University of Hong Kong, Pokfulam Road, Hong Kong, China

(Received 12 November 2020; accepted 2 March 2021; published 26 March 2021)

A 40-year-old puzzle in transition metal pentatellurides $ZrTe_5$ and $HfTe_5$ is the anomalous peak in the temperature dependence of the longitudinal resistivity, which is accompanied by sign reverses of the Hall and Seebeck coefficients. We give a plausible explanation for these phenomena without assuming any phase transition or strong interaction effect. We show that, due to intrinsic thermodynamics and diluteness of the conducting electrons in these materials, the chemical potential displays a strong dependence on the temperature and magnetic field. With that, we compute resistivity, Hall and Seebeck coefficients in zero field, and magnetoresistivity and Hall resistivity in finite magnetic fields, in all of which we reproduce the main features that are observed in experiments.

DOI: 10.1103/PhysRevLett.126.126601

Introduction.—A 40-year-old puzzle in transition metal pentatellurides $ZrTe_5$ and $HfTe_5$ is the anomalous peak in the temperature dependence of resistivity and the accompanying sign reverses of Hall and Seebeck coefficients [1–5]. The peak temperature T_p varies in the range 0–200 K in different samples. Early attempts to explain these transport anomalies through a structural transition or charge and spin density waves failed [6,7]. A recent theoretical proposal [8] that they are good candidates of topological insulators or Weyl semimetals has motivated a great effort to reinvestigate the two materials, leading to many interesting discoveries, such as the chiral magnetic effect [9] and 3D quantum Hall effects [10]. Regarding the puzzle, important progress was made by angle-resolved photoemission spectroscopy (ARPES) experiments [11,12] (see also Refs. [13–15]): it was observed that, as temperature increases, the chemical potential shifted from the electronlike conduction band to the holelike valence band, consistent with the change of charge carrier type. This observation was attributed to the temperature-induced Lifshitz transition, but the underlying reason remains unclear. Other explanations to the puzzle are also proposed, such as polaronic models with strong electron-phonon coupling [16,17], bipolar conduction [18], semimetal-semiconductor transition [19], or topological phase transition [20,21]. So far, the problem is still under debate.

In this Letter, we show that the above puzzle can be well resolved by intrinsic thermodynamics of noninteracting electrons, without the need of a phase transition or strong interaction. One of our key observations is that there are two small energies in $ZrTe_5$ and $HfTe_5$: the Fermi energy E_F and a particle-hole (PH) symmetry breaking energy Δ. The latter implies that the density of states (DOS) becomes very asymmetric between the conduction and valence bands for energy bigger than Δ. Estimates from experiments are $E_F = 15$–40 and $\Delta = 30$–40 meV. We show that the smallness of E_F and Δ makes the chemical potential highly sensitive to the temperature T and external magnetic field B, leading to the experimentally observed chemical potential shift [11,12]. With this thermodynamic property and the Kubo formula, we are able to reproduce the main transport features observed in experiments, including the resistivity peak and sign reverses of the Hall and Seebeck coefficients.

Model.—Our discussions will focus on $ZrTe_5$ but they can be easily adapted to $HfTe_5$. $ZrTe_5$ is a highly anisotropic layered material. According to Ref. [11], the low-energy band structure contains a Dirac-like electron pocket at Γ point and four other electron pockets near the Brillouin zone boundary. We model them by an anisotropic Dirac fermion and four identical anisotropic quadratic fermions [Fig. 1(a)]. The Dirac fermion has the well-known relativistic dispersion $E = \pm\sqrt{m^2 + v_x^2 p_x^2 + v_y^2 p_y^2 + v_z^2 p_z^2}$, where m is the Dirac mass and v_α is the velocity in α direction, $\alpha = x, y, z$. The energy bottom of the quadratic fermions is Δ, measured from the midpoint of the Dirac

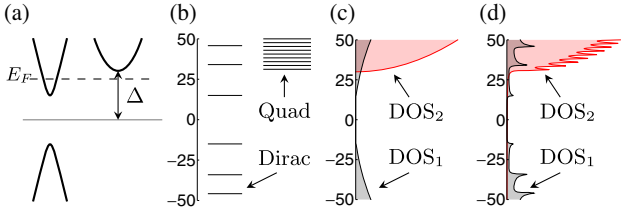

FIG. 1. (a) Schematics of the low-energy band structure in $ZrTe_5$. (b) Landau level bottoms of 3D Dirac and quadratic fermions with $B = 4$ T (energy in units of meV; see Fig. 2 for numerics). (c) Densities of states at $B = 0$ and (d) at $B = 4$ T (smoothed by a small disorder).

dispersion. For the Dirac and quadratic fermions, densities of states per volume are given, respectively, by

$$D_1(\epsilon) = 2\alpha_1|\epsilon|\sqrt{\epsilon^2 - m^2}\Theta(|\epsilon| - m),$$
$$D_2(\epsilon) = 2\kappa\alpha_2\sqrt{\epsilon - \Delta}\Theta(\epsilon - \Delta), \quad (1)$$

where $\alpha_1 = 1/(2\pi^2\hbar^3 v_x v_y v_z)$, $\Theta(x)$ is the Heaviside step function, $\kappa = 4$ denotes the four copies of quadratic fermions, $\alpha_2 = \sqrt{2m_x^* m_y^* m_z^*}/(2\pi^2\hbar^3)$, m_α^* is the anisotropic effective mass of quadratic fermions, and the factor 2 comes from spin degeneracy. The total DOS is $D(\epsilon) = D_1(\epsilon) + D_2(\epsilon)$. We emphasize that the Dirac dispersion is PH symmetric, i.e., $D_1(\epsilon) = D_1(-\epsilon)$. The presence of the quadratic fermions breaks the PH symmetry.

We also consider the effect of an external magnetic field $\mathbf{B} = B\hat{z}$, under which electron eigenstates form Landau levels. Details on Landau levels of the Dirac fermion can be found, e.g., in Refs. [22,23] or the Supplemental Material [24]. The Landau level energy is given by $E_a = \lambda\sqrt{m^2 + \hbar^2\omega_{c1}^2 N + v_z^2 p_z^2}$, where $N \geq 0$ is the Landau level index, p_z is the momentum along z direction, $\lambda = \pm 1$ represents the electron or hole branch, respectively, $\omega_{c1} = \sqrt{2v_x v_y eB/\hbar c}$ is relativistic cyclotron frequency, and Zeeman splitting is neglected. Landau levels of quadratic fermions are textbook results, with the energy $E = \hbar\omega_{c2}(N + 1/2) + p_z^2/2m_z^* + \Delta$, where $\omega_{c2} = eB/(c\sqrt{m_x^* m_y^*})$. The densities of states are now given by

$$D_1(\epsilon, B) = \alpha_1 \sum_{N\geq 0} \frac{d_N \hbar^2\omega_{c1}^2|\epsilon|}{2\sqrt{\epsilon^2 - E_{N1}^2}}\Theta(|\epsilon| - E_{N1}),$$
$$D_2(\epsilon, B) = \kappa\alpha_2 \sum_{N\geq 0} \frac{\hbar\omega_{c2}}{\sqrt{\epsilon - E_{N2}}}\Theta(\epsilon - E_{N2}), \quad (2)$$

where $d_N = 2 - \delta_{N,0}$, $E_{N1} = \sqrt{m^2 + \hbar^2\omega_{c1}^2 N}$, and $E_{N2} = \hbar\omega_{c2}(N + 1/2) + \Delta$. The latter two are the bottom energies of 3D Landau levels of the Dirac and quadratic fermions, respectively. In the limit $B \to 0$, expressions in (2) reduce to those in (1).

Figure 1(b) plots the Landau level bottoms at $B = 4$ T to give readers a sense of level spacings, with numerics given in the caption of Fig. 2. We note that the Dirac fermion is "lighter" than the quadratic fermions and thereby has bigger level spacings. Figures 1(c) and 1(d) show densities of states in zero field and in a finite B field, respectively. Effect of disorder is neglected in our thermodynamic calculations. It will be included in our calculations of transport properties below.

Chemical potential $\mu(T, B)$.—With the above densities of states, we now study the T and B dependence of the chemical potential μ. The particle number density $n(T, B, \mu)$ can be expressed as

$$n(T, B, \mu) = \int_0^\infty d\epsilon D(\epsilon, B) f_T(\epsilon - \mu) + \int_{-\infty}^0 d\epsilon D(\epsilon, B)[f_T(\epsilon - \mu) - 1], \quad (3)$$

where $f_T(\epsilon) = 1/[\exp(\epsilon/T) + 1]$ is the Fermi-Dirac distribution (Boltzmann constant k_B is absorbed into T throughout the Letter). Charge neutrality is taken to be at $\epsilon = 0$. The density n is fixed in a given 3D sample, so Eq. (3) should be understood as an integral equation that defines a function $\mu(T, B)$.

We solve Eq. (3) numerically by setting all the parameters in (1) and (2) to be comparable to experimentally measured values [10]. The results are shown in Fig. 2. When T varies in the range 0–25 meV and B varies in the range 0–25 T, our calculation shows a significant variation in μ, of the order of E_F, in agreement with the ARPES

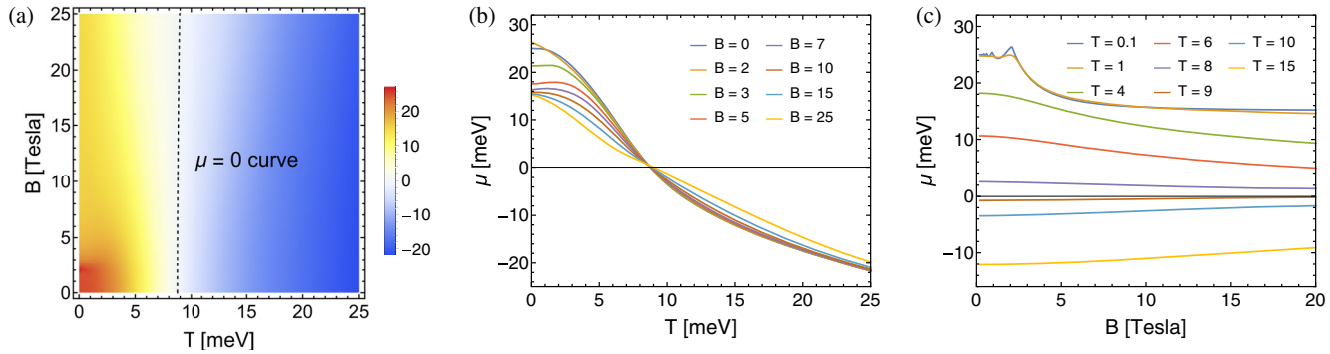

FIG. 2. Plots of the chemical potential μ versus temperature T and magnetic field B, obtained from Eq. (3) with parameters set approximately to the experimental values in Refs. [10,11]: $E_F = 25$ meV, $m = 15$ meV, $\Delta = 30$ meV, $\hbar v_x = 6.0$ eV Å, $\hbar v_y = 1.3$ eV Å, $\hbar v_z = 0.2$ eV Å, $m_x^* = m_y^* = 0.2m_e$, $m_z^* = 2m_e$, with m_e being the electron mass. The effective masses m_x^*, m_y^*, m_z^* of the quadratic fermions have not been measured experimentally to our knowledge, so they are set to typical values with anisotropy taken into account. The associated number density is $n = 1.73 \times 10^{17}$ cm^{-3}, and cyclotron energies are $\hbar\omega_{c1} = 15.3\sqrt{B}$ and $\hbar\omega_{c2} = 2.4B$ meV. (a) Color plot of $\mu(T, B)$. (b) T dependence of μ for several fixed B's. (c) B dependence of μ for several fixed T's. Numerical data in other figures are the same as here if not otherwise specified.

observation [11]. In particular, for $B = 0$, the chemical potential μ decreases monotonically from a positive E_F into a negative value around $T_0 \approx 10$ meV. One can show that this monotonic decreasing behavior occurs for a fairly general class of densities of states—see Supplemental Material [24]. A monotonic behavior is also observed when $T \gtrsim \hbar\omega_{c1}$ for a finite B. When $T \lesssim \hbar\omega_{c1}$, quantum oscillations in μ can also be seen in Fig. 2(c), which, however, is not our focus.

The fact that μ changes so dramatically compared to conventional metals in the temperature regime $T \lesssim 25$ meV and in experimentally accessible magnetic fields $B \lesssim 25$ T follows from two properties of $ZrTe_5$: (i) E_F is small, approximately 25 meV, i.e., conducting electrons are dilute, and (ii) the PH symmetry is broken at the energy scale of Δ, and $\Delta \approx E_F$. Generally speaking, variation of μ is set by T/E_F and $\hbar\omega_{c1}/E_F$. Accordingly, a small E_F makes it easier to achieve a significant change in μ by tuning T and B. Nevertheless, without property (ii), one can show that the PH symmetry guarantees $\mu > 0$, if $E_F > 0$. Or equivalently, PH symmetry pushes the sign-reversing temperature T_0, defined by $\mu(T_0, B) = 0$, to infinity. To have a finite T_0, the PH symmetry must be broken. We will show below that T_0 is closely related to the sign-reversing temperature of the Hall and Seebeck coefficients. While the scale of T_0 is set by Δ, its precise value depends on E_F, the effective masses m_α^*, magnetic field B, etc. We note that, in Fig. 2(b), T_0 barely displays a dependence on B. However, there is actually a very weak quadratic correction, $\delta T_0 \propto B^2$, which we discuss in the Supplemental Material [24]. We remark that a nonzero Dirac mass m is not important. Very similar behaviors of μ and transport properties are obtained for $m = 0$ (see Supplemental Material [24] for more discussions).

Resistivity, Hall and Seebeck coefficients.—We now proceed to calculate transport coefficients and see if the above thermodynamic behaviors can result in the experimentally observed resistivity peak and other transport phenomena. We begin with the longitudinal resistivity $\rho_{xx}(T)$, Hall coefficient $R_H(T)$, and Seebeck coefficient $S_{xx}(T)$ in zero magnetic field. Below, we only discuss transport properties in electron-doped systems (i.e., $E_F > 0$). Zero-field transport in hole-doped systems is discussed in the Supplemental Material [24].

To calculate transport coefficients, we use the Kubo formula (see, e.g., Refs. [27,28]). Our calculations are standard and details are included in the Supplemental Material [24]. The Hall coefficient, defined by $\rho_{yx} = R_H B$, is obtained by taking the $B \to 0$ limit of our finite-magnetic-field results. The Seebeck coefficient is computed by a generalized Mott formula that was obtained in Ref. [29]. Here, we discuss how disorder is treated. Disorder is the *only* source of resistivity in our calculations, as electron-phonon and electron-electron scattering are absent. It is included by an energy level broadening Γ_a in the single-particle Green's function

$$G_a(\omega) = \frac{1}{\omega - E_a + i\Gamma_a(\omega)}, \tag{4}$$

where E_a is the energy associated with the single-particle eigenstate $|a\rangle$. We take a crude simplification: $\Gamma_a(\omega) = \Gamma_1$ is a constant for all eigenstates of the Dirac fermion, and $\Gamma_a(\omega) = \Gamma_2$ is also a constant for all eigenstates of the quadratic fermions. We will see that this somewhat oversimplified treatment produces surprisingly good results. In the Supplemental Material [24], we also apply the Born approximation [28] of disorder for zero-field transport quantities as a comparison, but no qualitative difference is observed. Therefore, we will not bother to apply more realistic disorder models at finite B fields where self-consistent Born approximation may be necessary for large B [30].

Evaluations of $\rho_{xx}(T)$, $R_H(T)$, and $S_{xx}(T)$ are done numerically with an input of temperature-dependent μ determined from Eq. (3). The results are shown in Fig. 3. Indeed, an anomalous peak appears in the longitudinal resistivity and the sign reverses in both the Hall and Seebeck coefficients, all of which occur around the temperature T_0. The shapes of the curves in Figs. 3(a), 3(c), and 3(e) agree very well with those in experiments [1–5,10,15,31]. To have a better understanding, we show different contributions to the longitudinal conductivity σ_{xx} and Hall conductivity σ_{xy} in Figs. 3(b) and 3(d). Contributions from intrabranch scatterings of the Dirac fermion ($\sigma^{(1)}_{\alpha\beta,e}$ and $\sigma^{(1)}_{\alpha\beta,h}$) dominate, and those from interbranch scattering $\sigma^{(1)}_{\alpha\beta,eh}$ and the quadratic fermions $\sigma^{(2)}_{\alpha\beta}$ are negligible in the temperature regime of our interests. Intuitively, the "relativistic" Dirac fermion moves much faster than the "nonrelativistic" quadratic fermions, and so contributes more to the conductivity [32]. Although they do not conduct much current, the quadratic fermions do serve as good thermodynamic reservoirs, as shown in Fig. 3(f). That is, they are thermodynamically activated, but not quite in transport.

Analytically, once we neglect the contributions from the quadratic fermions and interbranch scattering of the Dirac fermion and focus on the regime $T \gg \Gamma_1$, the conductivities can be approximated by

$$\sigma_{xx} \approx C_{xx} \sum_{\lambda=\pm} \int_m^\infty d\epsilon \frac{(\epsilon^2 - m^2)^{3/2}}{\epsilon} [-f_T'(\lambda\epsilon - \mu)],$$
$$\sigma_{xy} \approx C_{xy} \sum_{\lambda=\pm} \int_m^\infty d\epsilon \frac{(\epsilon^2 - m^2)^{3/2}}{\epsilon^2} [\lambda f_T'(\lambda\epsilon - \mu)], \tag{5}$$

where the coefficients are $C_{xx} = v_x^2 \alpha_1 \hbar e^2/(3\Gamma_1)$ and $C_{xy} = e^3 \hbar^2 B v_x^2 v_y^2 \alpha_1/(6c\Gamma_1^2)$. The conductivity σ_{yy} can be obtained by replacing the index "x" with "y" in the

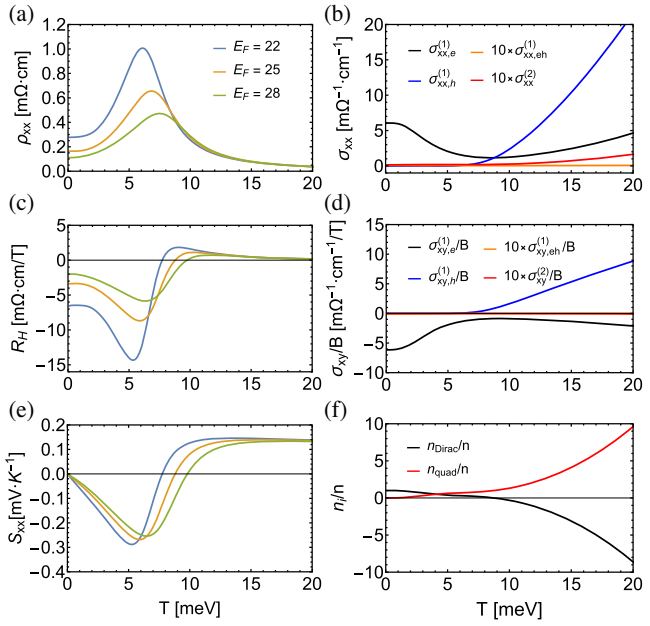

FIG. 3. Temperature dependence of the longitudinal resistivity (a) ρ_{xx}, (c) Hall coefficient R_H, and (e) Seebeck coefficient S_{xx} with different Fermi energies. The level broadening constants are set by $\Gamma_1 = 0.5$ meV (estimated from experimental data in Ref. [10]) and $\Gamma_2 = 10\Gamma_1$ (see an estimate in the Supplemental Material [24] using Born approximation) throughout our calculations. (b),(d) Different contributions to the longitudinal conductivity σ_{xx} and Hall conductivity σ_{xy} at $E_F = 25$ meV. (f) The density ratios n_{Dirac}/n and n_{quad}/n versus temperature.

expression of σ_{xx}, and the resistivity is given by $\rho_{\alpha\beta} = (\sigma^{-1})_{\alpha\beta}$. One can see that, when $\mu = 0$, the Hall conductivity σ_{xy} is zero, which is a consequence of the PH symmetry of the Dirac fermion. The nonzero conductivity $\sigma_{xy}^{(2)}$, though tiny, makes the sign-reversing temperature $\tilde{T}_0$ of R_H differ slightly away from the sign-reversing temperature T_0 of μ.

Magnetoresistivity and Hall resistivity at finite B.—The longitudinal resistivity $\rho_{xx}(T, B)$ and Hall resistivity $\rho_{yx}(T, B)$ in a finite magnetic field B are also calculated. The calculation is similar to the zero-field case: we first express the Kubo formula of the conductivity tensor $\sigma_{\alpha\beta}$ in the Landau level basis, then input the chemical potential $\mu(T, B)$ obtained from Eq. (3), and finally evaluate the conductivity numerically (see details in the Supplemental Material [24]).

Numerical results are shown in Fig. 4. Our focus is the high-field and high-temperature regime, i.e., T, $\hbar\omega_{c1} \gtrsim \Gamma_1$. The curves of ρ_{xx} and ρ_{yx} as functions of T or B again show good agreement with experiments. Two features deserve some attention. First, the "anomalous" peak in $\rho_{xx}(T)$ is largely enhanced by the magnetic field, which was initially observed in experiments in Ref. [33] (see also [10,31]). Theoretically, current conduction occurs when electrons and/or holes hop between two states, in the Nth and $(N+1)$th Landau levels, respectively, whose energies overlap after disorder broadening. By increasing B such that Landau level spacing is larger than Γ_1, available states that overlap in energy greatly decrease, leading to enhancement of resistivity. For the same reason, ρ_{yx} is also enlarged by the magnetic field. Second, the temperature $\tilde{T}_0$ at which $\sigma_{xy} = 0$ (equivalently, $\rho_{yx} = 0$) increases as B increases (e.g., see experiments in Refs. [10,31]). When B is large, $\sigma_{xy}^{(2)}$ cannot be neglected, as shown in the inset of Fig. 4(b). The underlying reason is that Landau level spacing is much smaller for the quadratic fermions than for the Dirac fermion, so $\sigma_{xy}^{(1)}$ reduces faster than $\sigma_{xy}^{(2)}$ as B increases. If $\sigma_{xy}^{(2)}$ is neglected, $\sigma_{xy} = 0$ occurs at $\mu = 0$ and so $\tilde{T}_0 = T_0$, which has negligible B dependence. Now that $\sigma_{xy}^{(2)}$ is non-negligible, its B dependence as well as the B dependence of other conductivity contributions make $\tilde{T}_0$ increase as B increases. This is also the reason behind the feature that $\rho_{yx}(B)$ reverses the sign as B increases, for certain temperatures, as shown in Fig. 4(d).

Discussions.—In summary, we have proposed a mechanism for the long-standing transport anomaly in dilute metals $ZrTe_5$ and $HfTe_5$. Our proposal describes a scenario that a minority current carrier may be thermodynamically very active, leading to intriguing interplay between equilibrium thermodynamics and transport properties. Many aspects of this work can be improved, e.g., by a more

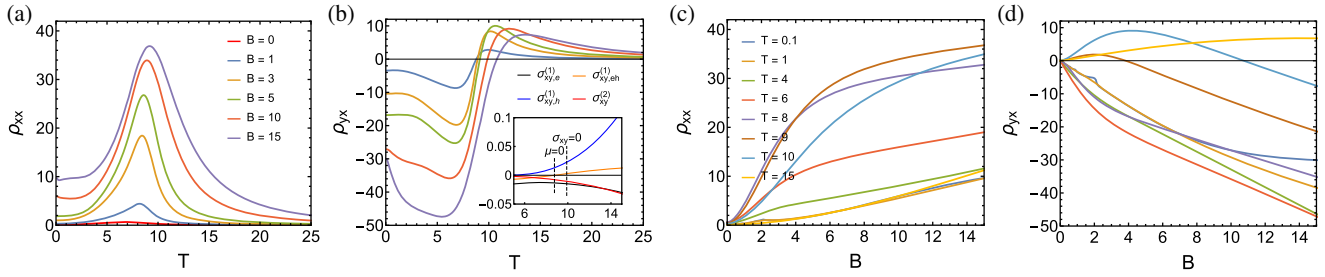

FIG. 4. Calculated magnetoresistivity and Hall resistivity. (a),(b) Temperature dependences of magnetoresistivity ρ_{xx} and Hall resistivity ρ_{yx} in various magnetic fields. (c),(d) Magnetic-field dependences of ρ_{xx} and ρ_{yx} at various temperatures. Inset in (b) shows different contributions to $\sigma_{xy}(T)$ at $B = 10$ T. The dashed lines mark the temperatures at which $\mu = 0$ and $\sigma_{xy} = 0$, respectively. Units of all numerics are the same as in Fig. 3.

realistic handling of disorder and by including electron-phonon coupling in the high-temperature regime. However, we believe that our model captures the essence of the experimentally observed transport anomalies. In the present model, the quadratic bands are responsible for PH symmetry breaking. However, in real samples there exist other factors that break PH symmetry, e.g., additional electron pockets [34] or the Dirac band itself being asymmetric [17]. Hence, detailed experimental or first-principles study on the asymmetry of low-energy band structure is strongly encouraged for the purpose of verifying or falsifying our theory at a more quantitative level. This work can be thought of as a microscopic theory of the phenomenological multicarrier model that is commonly used to fit experimental data [10,15,31]. For future studies, it would be interesting to extend this work to other dilute metals, such as $SrTiO_3$ [35].

C. W. acknowledges Liyuan Zhang for introducing the problem studied in this Letter and for various enlightening discussions, without whom this work would never have occurred. C. W. is grateful to Shizhong Zhang for encouragement and helpful discussions, and to Shun-Qing Shen for valuable discussions and for sharing his manuscript before publication. This work was supported by Research Grant Council of Hong Kong (ECS 21301018 and GRF 11300819) and URC, HKU (Grant No. 201906159002).

*cjwang@hku.hk

[1] T. J. Wieting, D. U. Gubser, S. A. Wolf, and F. Levy, Giant anomalies in the resistivities of quasi-one-dimensional $ZrTe_5$ and $HfTe_5$, Bull. Am. Phys. Soc. **25**, 340 (1980).
[2] S. Okada, T. Sambongi, and M. Ido, Giant resistivity anomaly in $ZrTe_5$, J. Phys. Soc. Jpn. **49**, 839 (1980).
[3] M. Izumi, K. Uchinokura, E. Matsuura, and S. Harada, Hall effect and transverse magnetoresistance in a low-dimensional conductor $HfTe_5$, Solid State Commun. **42**, 773 (1982).
[4] T. E. Jones, W. W. Fuller, T. J. Wieting, and F. Levy, Thermoelectric power of $HfTe_5$ and $ZrTe_5$, Solid State Commun. **42**, 793 (1982).
[5] D. N. McIlroy, S. Moore, D. Zhang, J. Wharton, B. Kempton, R. Littleton, M. Wilson, T. M. Tritt, and C. G. Olson, Observation of a semimetal–semiconductor phase transition in the intermetallic $ZrTe_5$, J. Phys. Condens. Matter **16**, L359 (2004).
[6] F. J. DiSalvo, R. M. Fleming, and J. V. Waszczak, Possible phase transition in the quasi-one-dimensional materials $ZrTe_5$ or $HfTe_5$, Phys. Rev. B **24**, 2935 (1981).
[7] S. Okada, T. Sambongi, M. Ido, Y. Tazuke, R. Aoki, and O. Fujita, Negative evidences for charge/spin density wave in $ZrTe_5$, J. Phys. Soc. Jpn. **51**, 460 (1982).
[8] H. Weng, X. Dai, and Z. Fang, Transition-Metal Pentatelluride $ZrTe_5$ and $HfTe_5$: A Paradigm for Large-Gap Quantum Spin Hall Insulators, Phys. Rev. X **4**, 011002 (2014).
[9] Q. Li, D. E. Kharzeev, C. Zhang, Y. Huang, I. Pletikosić, A. V. Fedorov, R. D. Zhong, J. A. Schneeloch, G. D. Gu, and T. Valla, Chiral magnetic effect in $ZrTe_5$, Nat. Phys. **12**, 550 (2016).
[10] F. Tang, Y. Ren, P. Wang, R. Zhong, J. Schneeloch, S. A. Yang, K. Yang, P. A. Lee, G. Gu, Z. Qiao, and L. Zhang, Three-dimensional quantum Hall effect and metal-insulator transition in $ZrTe_5$, Nature (London) **569**, 537 (2019).
[11] Y. Zhang *et al.*, Electronic evidence of temperature-induced Lifshitz transition and topological nature in $ZrTe_5$, Nat. Commun. **8**, 15512 (2017).
[12] Y. Zhang *et al.*, Temperature-induced Lifshitz transition in topological insulator candidate $HfTe_5$, Sci. Bull. **62**, 950 (2017).
[13] R. Wu, J.-Z. Ma, S.-M. Nie, L.-X. Zhao, X. Huang, J.-X. Yin, B.-B. Fu, P. Richard, G.-F. Chen, Z. Fang, X. Dai, H.-M. Weng, T. Qian, H. Ding, and S. H. Pan, Evidence for Topological Edge States in a Large Energy Gap near the Step Edges on the Surface of $ZrTe_5$, Phys. Rev. X **6**, 021017 (2016).
[14] L. Moreschini, J. C. Johannsen, H. Berger, J. Denlinger, C. Jozwiak, E. Rotenberg, K. S. Kim, A. Bostwick, and M. Grioni, Nature and topology of the low-energy states in $ZrTe_5$, Phys. Rev. B **94**, 081101(R) (2016).
[15] H. Chi, C. Zhang, G. Gu, D. E. Kharzeev, X. Dai, and Q. Li, Lifshitz transition mediated electronic transport anomaly in bulk $ZrTe_5$, New J. Phys. **19**, 015005 (2017).
[16] M. Rubinstein, $HfTe_5$ and $ZrTe_5$: Possible polaronic conductors, Phys. Rev. B **60**, 1627 (1999).
[17] B. Fu, H.-W. Wang, and S.-Q. Shen, Dirac Polarons and Resistivity Anomaly in $ZrTe_5$ and $HfTe_5$, Phys. Rev. Lett. **125**, 256601 (2020).
[18] P. Shahi, D. J. Singh, J. P. Sun, L. X. Zhao, G. F. Chen, Y. Y. Lv, J. Li, J.-Q. Yan, D. G. Mandrus, and J.-G. Cheng, Bipolar Conduction as the Possible Origin of the Electronic Transition in Pentatellurides: Metallic vs Semiconducting Behavior, Phys. Rev. X **8**, 021055 (2018).
[19] D. N. McIlroy, S. Moore, D. Zhang, J. Wharton, B. Kempton, R. Littleton, M. Wilson, T. M. Tritt, and C. G. Olson, Observation of a semimetal-semiconductor phase transition in the intermetallic $ZrTe_5$, J. Phys. Condens. Matter **16**, L359 (2004).
[20] L.-X. Zhao, X.-C. Huang, Y.-J. Long, D. Chen, H. Liang, Z.-H. Yang, M.-Q. Xue, Z.-A. Ren, H.-M. Weng, Z. Fang, X. Dai, and G.-F. Chen, Anomalous magneto-transport behavior in transition metal pentatelluride $HfTe_5$, Chin. Phys. Lett. **34**, 037102 (2017).
[21] B. Xu, L. X. Zhao, P. Marsik, E. Sheveleva, F. Lyzwa, Y. M. Dai, G. F. Chen, X. G. Qiu, and C. Bernhard, Temperature-Driven Topological Phase Transition and Intermediate Dirac Semimetal Phase in $ZrTe_5$, Phys. Rev. Lett. **121**, 187401 (2018).
[22] A. H. Castro Neto, F. Guinea, N. M. R. Peres, K. S. Novoselov, and A. K. Geim, The electronic properties of graphene, Rev. Mod. Phys. **81**, 109 (2009).
[23] S.-Q. Shen, *Topological Insulators: Dirac Equation in Condensed Matter*, 2nd ed. (Springer, Singapore, 2017).
[24] See Supplemental Material at http://link.aps.org/supplemental/10.1103/PhysRevLett.126.126601 for technical analyses on $\mu(T, B)$, methods for computing transport coefficients, and additional discussion on zero-field transport, which includes Refs. [25,26].

[25] T. Liang, J. Lin, Q. Gibson, S. Kushwaha, M. Liu, W. Wang, H. Xiong, J. A. Sobota, M. Hashimoto, P. S. Kirchmann, Z.-X. Shen, R. J. Cava, and N. P. Ong, Anomalous Hall effect in $ZrTe_5$, Nat. Phys. **14**, 451 (2018).

[26] P. Zhang, R. Noguchi, K. Kuroda, C. Lin, K. Kawaguchi, K. Yaji, A. Harasawa, M. Lippmaa, S. Nie, H. Weng *et al.*, Observation and control of the weak topological insulator state in $ZrTe_5$, Nat. Commun. **12**, 406 (2021).

[27] G. D. Mahan, *Many-Particle Physics*, 3rd ed. (Springer, New York, 2000).

[28] G. Rickayzen, *Green's Functions and Condensed Matter* (Dover Publications, New York, 2013).

[29] M. Jonson and S. M. Girvin, Thermoelectric effect in a weakly disordered inversion layer subject to a quantizing magnetic field, Phys. Rev. B **29**, 1939 (1984).

[30] T. Ando, A. B. Fowler, and F. Stern, Electronic properties of two-dimensional systems, Rev. Mod. Phys. **54**, 437 (1982).

[31] Y. Liu, X. Yuan, C. Zhang, Z. Jin, A. Narayan, C. Luo, Z. Chen, L. Yang, J. Zou, X. Wu, S. Sanvito, Z. Xia, L. Li, Z. Wang, and F. Xiu, Zeeman splitting and dynamical mass generation in Dirac semimetal $ZrTe_5$, Nat. Commun. **7**, 12516 (2016).

[32] For a kinetic energy of 15 meV, quadratic fermions have a velocity $\hbar v_{x2} \approx \hbar\sqrt{2(15\ \mathrm{meV})/(3m_x^*)} \approx 0.6$ eV Å, compared to $\hbar v_{x1} \approx 6$ eV Å for the Dirac fermion.

[33] T. M. Tritt, N. D. Lowhorn, R. T. Littleton, A. Pope, C. R. Feger, and J. W. Kolis, Large enhancement of the resistive anomaly in the pentatelluride materials $HfTe_5$ and $ZrTe_5$ with applied magnetic field, Phys. Rev. B **60**, 7816 (1999).

[34] B. Monserrat and A. Narayan, Unraveling the topology of $ZrTe_5$ by changing temperature, Phys. Rev. Research **1**, 033181 (2019).

[35] S. Stemmer and S J. Allen, Non-Fermi liquids in oxide heterostructures, Rep. Prog. Phys. **81**, 062502 (2018).